Journal of Zhejiang University SCIENCE A
ISSN 1673-565X (Print); ISSN 1862-1775 (Online)
www.zju.edu.cn/jzus; www.springerlink.com
E-mail: jzus@zju.edu.cn

MRI and PET images fusion based on human retina model*

DANESHVAR Sabalan, GHASSEMIAN Hassan†‡

(*Department of Electrical and Computer Engineering, Tarbiat Modares University, P.O.Box 14115-143, Tehran, Iran*)

†E-mail: ghassemi@modares.ac.ir

Received Apr. 28, 2007; revision accepted Aug. 13, 2007

Abstract: The diagnostic potential of brain positron emission tomography (PET) imaging is limited by low spatial resolution. For solving this problem we propose a technique for the fusion of PET and MRI images. This fusion is a trade-off between the spectral information extracted from PET images and the spatial information extracted from high spatial resolution MRI. The proposed method can control this trade-off. To achieve this goal, it is necessary to build a multiscale fusion model, based on the retinal cell photoreceptors model. This paper introduces general prospects of this model, and its application in multispectral medical image fusion. Results showed that the proposed method preserves more spectral features with less spatial distortion. Comparing with hue-intensity-saturation (HIS), discrete wavelet transform (DWT), wavelet-based sharpening and wavelet-*à trous* transform methods, the best spectral and spatial quality is only achieved simultaneously with the proposed feature-based data fusion method. This method does not require resampling images, which is an advantage over the other methods, and can perform in any aspect ratio between the pixels of MRI and PET images.

Key words: Image fusion, Retina based, Multiresolution, Multiresolution image (MRI), Positron emission tomography (PET)
doi:10.1631/jzus.2007.A1624 **Document code:** A **CLC number:** TN911.73

INTRODUCTION

In medicine, the use of multi-modality images representing various functions has become a more general practice. Images of different modalities, when fused together, provide essential information for clinical diagnosis and prognosis. Good image quality can provide more reliable patient information, which can then be used for accurate clinical decision making. With the availability of multisensor images in many fields, fusion has emerged as a new and promising research area (Goshtasby and Nikolov, 2007). Multisensor image fusion generates a single image containing a more accurate description than any individual source image.

Image fusion algorithms can be categorized into low, mid, and high levels. In some literature, this is referred to as pixel, feature, and symbolic levels. Pixel-level algorithms work either in the spatial domain or in the transform domain (Toet, 1990; Nikolov *et al*., 2001; Goshtasby, 2005). Although the pixel-level fusion is a local operation, the transform domain algorithms create the fused image globally. By changing a single coefficient in the transformed fused image, all (or a whole neighborhood of) image values in the spatial domain will change. As a result, in the process of enhancing properties in some image areas, undesirable artifacts may be created in other image areas. Zheng *et al*.(2007) described a method to reduce artifacts by minimizing the ratio of the spatial frequency error. Algorithms working in the spatial domain have the ability to focus on the desired area, with no effect in other areas. Multiresolution analysis is a popular method in the pixel-level fusion. Burt (1984) and Burt and Kolczynski (1993) used filters with increasing spatial extent to generate a sequence of images (pyramid) from each image, separating information observed at different resolutions. Then at each position in the transform image, the value in the pyramid showing the highest saliency was taken. An inverse transform of the composite image was used to create the fused image.

‡ Corresponding author

* Project (No. TMU 85-05-33) supported in part by the Iran Telecommunication Research Center (ITRC)

Petrovic and Xydeas (2004) used intensity gradients as a saliency measure. In a similar manner, various wavelet transforms can be used to fuse images. The discrete wavelet transform (DWT) has been used in many applications to fuse images. More recently, the dual-tree complex wavelet transform (DT-CWT), first proposed by Kingsbury (1999), was shown by Nikolov *et al*.(2001) and Lewis *et al*.(2004) to outperform most other grey-scale image fusion methods.

While considerable work has been done at the pixel-level image fusion, less work has been done at feature-level image fusion and symbolic-level image fusion. Feature-based algorithms typically segment the images into regions and fuse the regions using their various properties. Feature-based algorithms are usually less sensitive to signal-level noise. Toet (1990) first decomposed each input image into a set of perceptually relevant patterns. The patterns were then combined to create a composite image containing all relevant patterns. Nikolov *et al*.(2000) developed a technique that fuses images based on their multi-scale edge representations, using the wavelet transform proposed by Mallat and Zhong (1992). Another mid-level fusion algorithm was developed by Piella (2003), in which images are first segmented and the obtained regions are then used to guide the multiresolution analysis. High-level fusion algorithms combine image descriptions, for instance, in the form of relational graphs.

In this study, low-resolution multispectral positron emission tomography (PET) images are fused with a high-resolution panchromatic MRI images to achieve optimal resolution in the spatial and spectral domains. Several methods have existed to modulate lower resolution panchromatic images, such as the HIS, PCA and DWT, etc. However, those methods normally improve the spatial resolution while distorting the spectral composite, or preserve the spectral information while degrading the spatial structure. The retina-based fusion technique can better preserve the spectral and spatial information than others. Visual and statistical analyses showed that the proposed retina model significantly improves the fusion quality compared to conventional fusion techniques.

GENERAL IMAGE FUSION METHODS

Fusion with HIS transform

The widespread use of the HIS transform to merge images is based on its ability to separate the spectral information of an RGB composition in its two components, H and S, while isolating most of the spatial information in the I component (Choi, 2006). Several algorithms have been developed to allow the conversion of the color values (RGB) into values of intensity, hue, and saturation. Whatever algorithm is chosen, the HIS transform is always applied to an RGB composite. This implies that the fusion will be applied to groups of three bands of the multispectral image. As a result of this transformation, we obtain the new intensity, hue, and saturation components. The panchromatic image then replaces the intensity image. Before doing this, in order to minimize the modification of the spectral information of the fused multispectral image with respect to the original multispectral image, the histogram of the panchromatic image is matched with that of the intensity image. Applying the inverse transform, we obtain the fused RGB image, with the spatial detail of the panchromatic image being incorporated into it.

$$\begin{bmatrix} I \\ V_1 \\ V_2 \end{bmatrix} = \begin{bmatrix} 1/3 & 1/3 & 1/3 \\ -\sqrt{2}/6 & -\sqrt{2}/6 & \sqrt{2}/6 \\ 1/\sqrt{2} & -1/\sqrt{2} & 0 \end{bmatrix} \begin{bmatrix} R \\ G \\ B \end{bmatrix}, \quad (1)$$

$$H = \arctan(V_2 / V_1), \quad (2)$$

$$S = \sqrt{V_1^2 + V_2^2}, \quad (3)$$

where I is the intensity component, H the hue component, S the saturation component, V_1 and V_2 the intermediate variables. Fusion is performed by replacing I with MRI image. Finally, the fused image is obtained by performing the inverse HIS transform (Fig.1). The HIS transform based image fusion algorithm can preserve the same spatial resolution as the source panchromatic image but seriously distort the spectral information in the source multispectral image.

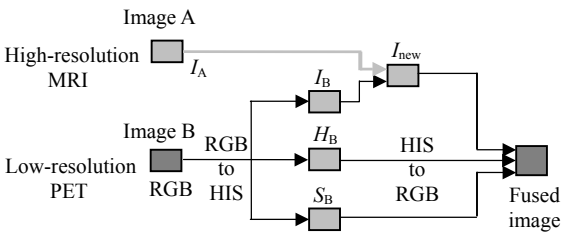

Fig.1 HIS fusion diagram

Fusion with DWT

One of the most widely used multiresolution strategies is the DWT. DWT is a linear transformation highly useful in the area of signal processing, where one of its principal applications consists in separating datasets into distinct frequency components, which are then represented on common scales. There are different forms of calculating the DWT in fusion algorithms. One of the most widely used algorithms is the pyramidal algorithm of (Mallat and Zhong, 1992), due to the high spectral quality of its resulting image, although its low anisotropic characteristic produces problems for the fusion of images with a high content of borders being not horizontal, vertical or diagonal.

Zhou *et al*.(1998) developed a DWT-based fusion algorithm to merge multispectral and panchromatic images. The source panchromatic image and each spectral band of the source multispectral image are decomposed into an orthogonal wavelet representation at a given coarser resolution, which consists of a low-frequency approximation image and a set of high-frequency images. Band-by-band, the fused images are derived by performing the inverse DWT using the approximation image from each band of the source multispectral image and detail images from the source panchromatic image (Fig.2). The performance of this fusion algorithm is better than those based on the HIS transform.

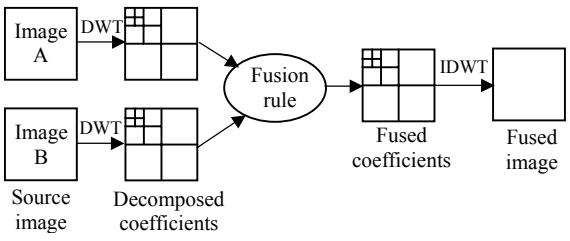

Fig.2 Schematic of the DWT-based fusion

Wavelet-based sharpening

The wavelet transform is a mathematical tool extensively used in image analysis and image fusion. Different wavelet-based pansharpening methods are available in (Nunez *et al*., 1999). In wavelet-based sharpening, the high frequency detail coefficients are obtained from the high spatial resolution panchromatic image and are combined with the spectral information obtained from the multispectral image through a combination model. The HIS transform or PCA transform is applied to the multispectral image as a preprocessing step. The intensity component (or the first principal component) is then used in the combination model. The process flow diagram of the wavelet-based sharpening technique is shown in Fig.3.

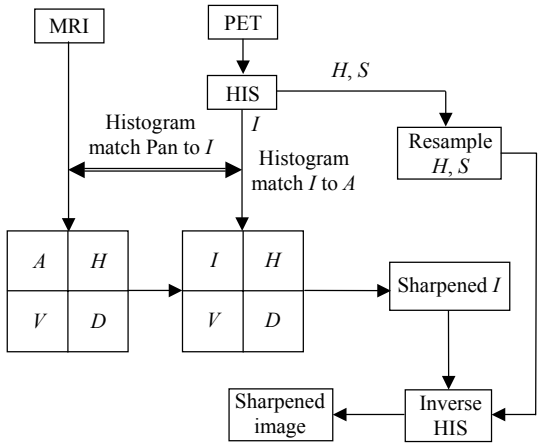

Fig.3 The fusion model based on wavelet-based sharpening (Zhou *et al*., 1998)

The multispectral image bands are first transformed into the HIS domain. The panchromatic image is histogram-matched with the intensity component. The histogram of the intensity component (I) is matched to the low-resolution approximation of the panchromatic image in the wavelet domain. The histogram-matched I component replaces the low-resolution component. The inverse wavelet transform is performed to obtain a fused intensity component where the high frequency details are added to the intensity component. The hue and saturation components are resampled to the size of the sharpened intensity band. The inverse HIS transformation is applied to get back to the RGB image domain.

Fusion with the wavelet-*à trous* algorithm

A wavelet *à trous* ("with holes") algorithm has been proposed by Joshi *et al*.(2006). This algorithm differs from the pyramidal ones in that it is redundant, which implies that between two successive levels, there is no dyadic spatial compression of the original image, but rather the image size is maintained. The basis of the pyramid represents the original image and each of its levels is a decomposed, compressed version of the image represented at the previous level.

In this way, spatial resolution and image size decrease from one level to the next. However, in wavelet *à trous* the spatial resolution decreases from one level to the next, but not the image size, which is constant for all levels. Comparative studies have shown that both the spatial and the spectral qualities of the fused images through the *à trous* algorithm are better than the ones provided by the Mallat algorithm.

The wavelet *à trous* algorithm consists basically in the application of consecutive convolutions between the image under analysis and a scaling function at distinct successive levels. One of the most widely used scaling functions for the computation of the *à trous* algorithm is the B3 Spline. If the original image without succession is represented by $I_j(x,y)$, the wavelet coefficients for the level $j+n$, $C_{j+n}(x,y)$, are obtained by the difference between the corresponding two consecutively decomposed images, $I_{j+n-1}(x,y)$ and $I_{j+n}(x,y)$, as shown in the following equation:

$$C_{j+n}(x,y) = I_{j+n}(x,y) - I_{j+n-1}(x,y). \quad (4)$$

To carry out image synthesis, from a successive level $j+n$, an additive criterion should be applied in which all the coefficients obtained are added to the last successive level of the original image, as represented by:

$$I_j(x,y) = I_{j+n}(x,y) + \sum_{k=1}^{n} C_{j+k}(x,y). \quad (5)$$

If $I_{j+n}(x,y)$ represents the successively decomposed planes that contain the low-frequency information of the original image, and $C_{j+n}(x,y)$ represents its respective wavelet coefficients, which contain the high-frequency information, then it is possible to plant an image fusion scheme. In this scheme, the low-frequency information contained in a multispectral image is fused with the high-frequency information contained in the wavelet coefficients of a high-resolution spatial image (panchromatic), to obtain a high spatial resolution multispectral image (Garzelli and Nencini, 2005).

RETINA MODEL

The retina is a thin layer of neural tissue in the back of the eye. It can be decomposed into five layers: three layers of cell bodies and two layers of synaptic interconnections between the neurons. This structural form is depicted in Fig.4. Light enters from the ganglion cell layer side first, and must penetrate all cell types before reaching the rods and cones. This is because the pigment-bearing membranes of the photoreceptors have to be in contact with the eye's pigment epithelial layer (Kolb, 1991). The photoreceptors' cell bodies are located in the outer nuclear layer of the retina. The synaptic terminals of the photoreceptors make contact with the dendritic fields of the bipolar cells and horizontal cells in the outer plexiform layer (OPL). The cell bodies of the bipolar and horizontal cells are located in the inner nuclear layer. The horizontal cells make connections with the cells in the outer nuclear layer. The bipolar cells, however, make connections onto the dendrites of the ganglion cells within the inner plexiform layer (IPL). Since only the bipolar cells link the signals in the outer and inner plexiform layers, all the visual signals must go through the bipolar cells. Another class of cells located in the inner nuclear layer is the amacrine cells. These cells have no identifiable axons, only dendrites. The dendritic fields of the amacrine and ganglion cells connect in the inner plexiform layer. The retinal ganglion cell bodies are located in the ganglion cell layer, and their dendritic fields connect with the axon terminals of the bipolars as well as with the dendritic fields of the amacrine cells.

Totally, OPL properties are generated by the synaptic triad, which is composed of three kinds of interconnected cells (Kolb, 1991):

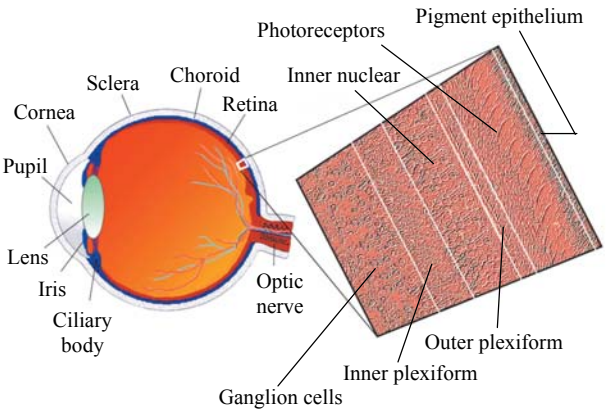

Fig.4 A thin piece of retina is enlarged in a photomicrograph revealing its layers (Kolb, 1991)

(1) The cone cells constitute a layer of the transduction and regularization processing. The transduction converts luminance into electrochemical potentials aimed at the downstream layers. The regularization consists in filtering input signals with a light low-pass frequencies filtering. The cone cells are defined by their shapes (midget, diffuse, …), their types of response (on, off) and their functions (spectral sensibilities: red, green, and blue colors). Moreover their behaviors depend locally on the luminance intensity and contrast.

(2) The horizontal cells constitute a layer of strong regularization processing. The output response performs from the cone cells output to elaborate a spatial average of the image intensity.

(3) The bipolar cells make the difference between the horizontal (luminance average) and the cone outputs. Therefore bipolar cells estimate the local contrasts of the image intensity to increase visual indices. As cone cells, the bipolar cells are various. We observe bipolar cells are classified also by their shapes (midget, diffuse, …), their types of response (bipolar on, off, …), and their functions (contrast estimation: red/green, blue/green+red, …).

The bipolar axons transmit the OPL outputs to the IPL area. The IPL processing is assumed by ganglion cells:

The ganglion cells have a receptive field organized as concentric circles. The ganglion cells are classified as bipolar cells by their shapes (midget, diffuse, ...), their types of response (on, off, on+off), and their functions (spatial contrast estimation and luminance estimation) (Kolb, 1991).

The biological computational processes of the human retina motivate our image fusion architectures. The three different cone cells in the retina are sensitive to the short, medium, and long wavelengths of the visible spectrum. If the retina was simply to transmit opposite-contrast images directly from the photoreceptors to the brain, the resulting vision would probably be coarse-grained and blurry. Further processing in the retina defines precise edges to images and allows us to focus on fine details. The honing of the image starts at the first synaptic level in the retina, where horizontal cells receive input from the cones.

The biological retina not only converts optical information into electrical signals but performs considerable processing on the visual signal before transmitting it to higher visual system levels. Image fusion can incorporate the processing principles of human vision system. This paper presents a multiresolution data fusion scheme, based on retinal visual channels decomposition, motivated by analytical results obtained from retina based image analysis. The energy packing the spectral features is distributed in the lower frequency subbands, while the spatial features and edges are distributed in the higher frequency subbands (Ghassemian, 2001b). By adding the high-scale spatial features (extracted from an MRI image) to the low-scale spatial features (from PET image), the visual-channel procedure enhances the multispectral images (see Fig.5).

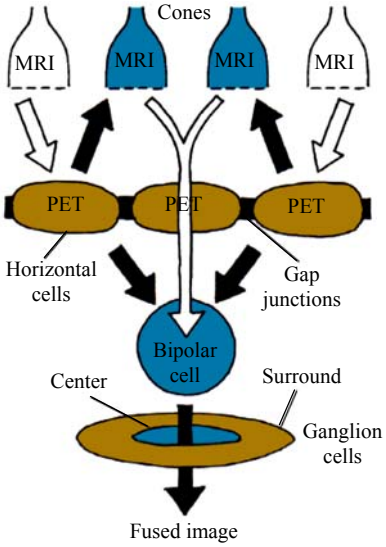

Fig.5 A multiscale image fusion scheme in the retina

The computer retina model presented is based on Difference-of-Gaussian (DoG) operator (Ghassemian, 2001a), which described some of the receptive field properties of the ganglion cells. It consists of two Gaussians with different variances at position (x,y) and can generally be written as:

$$CS(x,y)=\alpha_c G(r;\sigma_c)-\alpha_s G(r;\sigma_s), \tag{6}$$

$$G(r;\sigma)=\frac{1}{2\pi\sigma^2}\exp[-|r|^2/(2\sigma^2)], \tag{7}$$

where $r=\sqrt{x^2+y^2}$, α_c and α_s are weights of centre and surrounding inputs, G_{σ_c} and G_{σ_s} are normalized filters (a spatial integral of one) that represent the

filtering of the visual sequence taking place respectively in light receptors (G_{σ_c}, or center signal) and horizontal cells (G_{σ_s}, or surrounding signal). Both filters are spatially low-pass. Filter G_{σ_s} is more narrow than G_{σ_c} in the frequency domain, which means $\sigma_s > \sigma_c$. It corresponds to the biological fact that horizontal cells develop their signal with more synapses and more cellular integrations than receptors, and are linked to their neighboring horizontal cells through strongly coupling gap junctions.

In summary, the outputs from these photoreceptors are oppositely enhanced within band by center-surround spatial opponent processes at the bipolar cells. In later stages (ganglion cells in retina) these signals are oppositely enhanced by center-surround processes between the different bands.

Ultimately, we can represent the function of this model by (Ghassemian, 2001b):

$$f(x,y) = h_1(x,y) \otimes f_1(x,y) + h_2(x,y) \otimes f_2(x,y), \quad (8)$$

where $f_1(x,y)$ is the high-resolution image, $h_1(x,y)$ is the high-pass filter (photoreceptors cells), $f_2(x,y)$ is the low-resolution image and $h_2(x,y)$ is the low-pass filter (horizontal cells). This allows to generate a spatially enhancing multispectral image $f(x,y)$, by adding the high-resolution spatial features to $f_2(x,y)$.

EXPERIMENTAL RESULTS

The widespread use of multi-sensor and multispectral images in medical diagnostics has increased the importance of assessing the quality of different fusion techniques and relating it to human or computer performance. Better quality assessment tools are needed to compare results obtained by different fusion techniques and to derive the optimal parameters of these techniques. Often the ideally fused image is not known or is very difficult to construct. This makes it impossible to compare fused images to a gold standard. In applications where the fused images are for human observation, the performance of fusion algorithms can be measured in terms of improvement in user performance in tasks like detection, recognition, tracking, or classification. This approach requires a well-defined task for which quantitative measurements can be made to characterize human performance. However, this is usually time consuming and often means expensive experiments with human subjects.

In recent years, a number of computational image fusion quality assessment metrics have been proposed (Wang *et al*., 2005). Metrics that accurately relate to human observer performance are of great value but are very difficult to design and, thus, are not yet available at present. In order to objectively compare different image fusion algorithms, what we also need is publicly available multispectral or multisensor datasets that can be used to benchmark existing and new algorithms.

In this experiment, multispectral PET image is fused with the MRI data. The tests data consist of multispectral PET dataset images and panchromatic MRI dataset images. The image size is 256×256 pixels. The multispectral images are registered to the corresponding panchromatic images. All images were downloaded from Harvard University Medical School site (http://www.med.harvard.edu/AANLIB/home.html). The brain images are of three groups (normal axial, normal coronal and mild Alzeimer's disease images). Each PET image consists of three multispectral bands (red, green, and blue) and MRI image has a bond. The retina-based method is compared with the HIS, DWT, wavelet-based sharpening and *à trous* wavelet transform methods. Visual evaluation of the spectral composite images indicates that the HIS, DWT, wavelet-based sharpening and *à trous* wavelet transform methods change spectral of the composite images, which means the spectral features are distorted by these methods (Figs.6~8). The image fusion algorithms should not distort the spectral characteristics of the original multispectral data.

A good fusion scheme should preserve the spectral characteristics of the source multispectral image as well as the high spatial resolution characteristics of the source panchromatic image. In this paper, two evaluation criteria are used for quantitative assessment of the fusion performance. The spectral quality of a $P \cdot Q$ fused image can be measured by the discrepancy D_k at each band (Li *et al*., 2005):

$$D_k = \frac{1}{PQ} \sum_{x=1}^{P} \sum_{y=1}^{Q} \left| f_k(x,y) - g_k(x,y) \right|, \quad (9)$$

$$K=R, G, B,$$

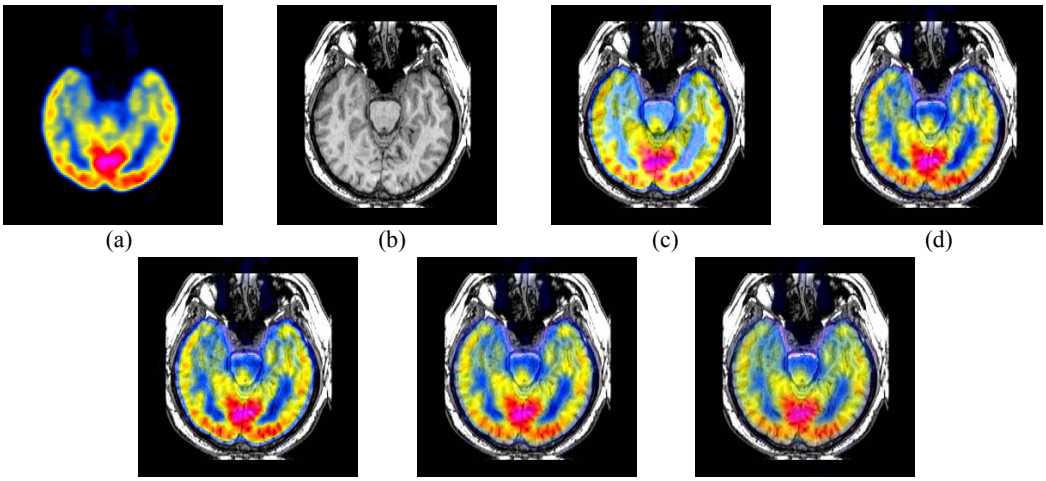

Fig.6 Original normal axial images and fused images (Dataset 1). (a) PET image; (b) MRI image; (c) HIS; (d) DWT; (e) Wavelet-based sharpening; (f) Wavelet-*à trous*; (g) Retina (proposed method)

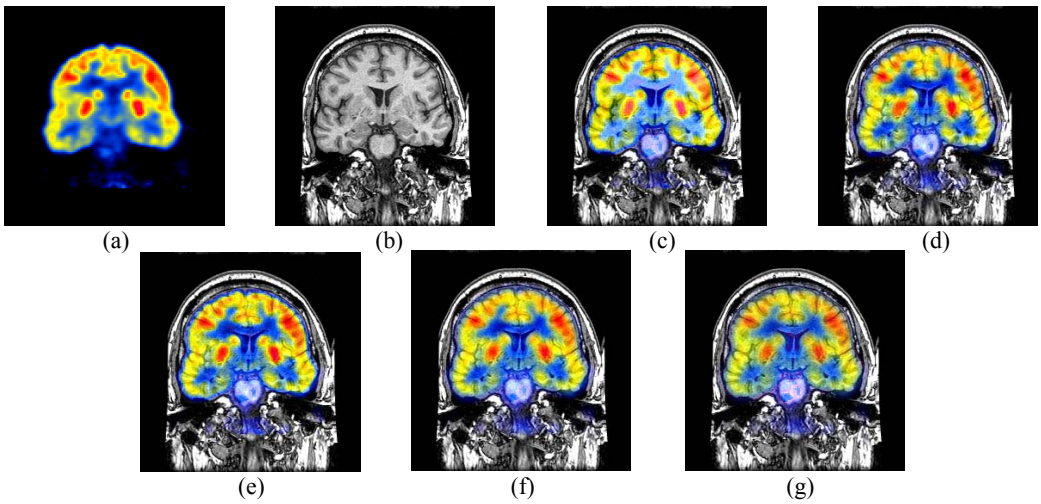

Fig.7 Original normal coronal images and fused images (Dataset 2). (a) PET image; (b) MRI image; (c) HIS; (d) DWT; (e) Wavelet-based sharpening; (f) Wavelet-*à trous*; (g) Retina (proposed method)

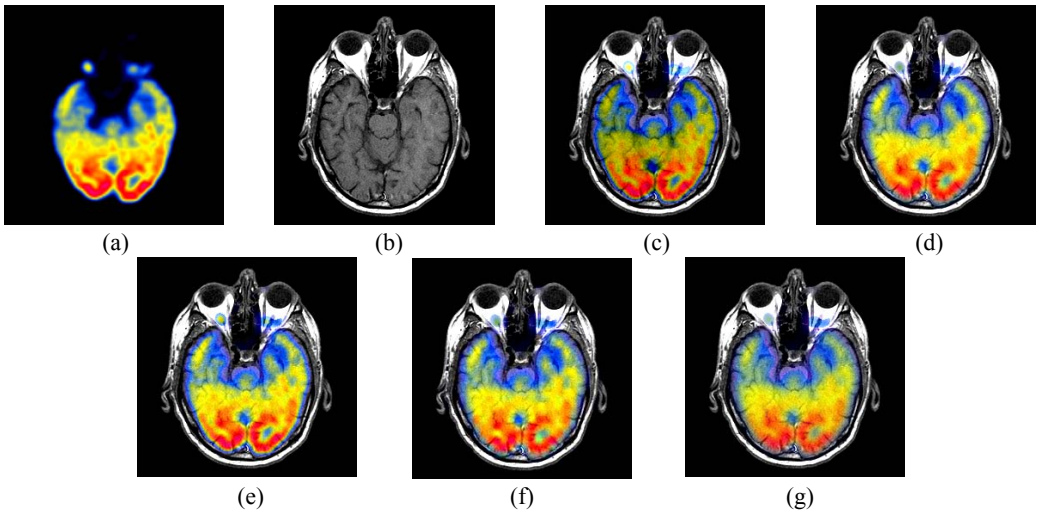

Fig.8 Original mild Alzeimer's disease images and fused images (Dataset 3). (a) PET image; (b) MRI image; (c) HIS; (d) DWT; (e) Wavelet-based sharpening; (f) Wavelet-*à trous*; (g) Retina (proposed method)

where $f_k(x,y)$ and $g_k(x,y)$ are the pixel values of the fused and original multispectral images at position (x,y), respectively; in this paper P=Q=256. A small discrepancy implies a good fusion result. For the spatial quality, we use the average gradient to evaluate the performance of the fused image (Ghassemian, 2001a), i.e.,

$$Avg_k = \sum_{x=1}^{P-1}\sum_{y=1}^{Q-1}\sqrt{\left[\left(\frac{\partial f_k(x,y)}{\partial x}\right)^2+\left(\frac{\partial f_k(x,y)}{\partial y}\right)^2\right]\Big/2} \cdot\frac{1}{(P-1)(Q-1)}, \quad k=R,G,B, \tag{10}$$

where $f_k(x,y)$ is the pixel value of the fused image at position (x,y). The average gradient reflects the clarity of the fused image. It can be used to measure the spatial resolution of the fused image, i.e., a larger average gradient means a higher spatial resolution.

Table 1 shows the spectral discrepancies between the images obtained by different fusion algorithms and the source multispectral image. The average gradients of the images obtained by different fusion algorithms are shown in Table 2. From these two tables, we can conclude that the proposed algorithm can preserve high spatial resolution characteristics of the source panchromatic image. In addition, the spectral distortion introduced to the proposed fusion method is less than those of the traditional algorithms based on the HIS, DWT, wavelet-based sharpening and *à trous* wavelet transform methods. Results showed that it preserves more spectral features with less spatial distortion.

Table 1 Spectral discrepancies between the fused images and the source multispectral image

Algorithm	Dataset 1				Dataset 2				Dataset 3			
	R	*G*	*B*	Avg.	*R*	*G*	*B*	Avg.	*R*	*G*	*B*	Avg.
HIS based algorithm	8.58	10.97	10.16	9.90	8.06	10.60	9.79	9.48	10.03	10.91	7.52	9.49
DWT based algorithm	7.14	7.28	10.12	8.18	6.74	7.71	11.07	8.51	5.20	6.47	8.05	6.57
Wavelet-based sharpening	9.31	8.09	11.50	9.63	9.06	8.12	12.07	9.75	7.22	6.75	8.96	7.64
Wavelet-*à trous* algorithm	6.40	6.66	9.16	7.40	6.01	7.10	9.86	7.66	4.67	5.70	7.26	5.88
The proposed algorithm	4.72	5.77	5.44	5.31	4.87	6.34	5.82	5.68	3.41	4.53	4.22	4.05

Table 2 Average gradients of the fused images

Algorithm	Dataset 1				Dataset 2				Dataset 3			
	R	*G*	*B*	Avg.	*R*	*G*	*B*	Avg.	*R*	*G*	*B*	Avg.
HIS based algorithm	3.33	3.82	5.60	4.25	3.58	4.16	5.33	4.36	2.94	3.27	3.80	3.34
DWT based algorithm	3.85	3.99	4.82	4.22	3.91	4.24	4.82	4.32	3.04	3.51	3.86	3.47
Wavelet-based sharpening	3.40	3.52	4.00	3.64	3.59	3.87	4.10	3.85	2.83	3.07	3.24	3.05
Wavelet-*à trous* algorithm	3.61	3.77	4.48	3.95	3.73	4.07	4.48	4.09	2.91	3.35	3.63	3.30
The proposed algorithm	3.98	4.40	5.78	4.72	4.08	4.71	5.77	4.85	3.18	3.90	4.73	3.93

CONCLUSION

In this paper we present a multiresolution image fusion scheme, based on retinal visual channels decomposition. Basically, after the registration steps, the high-frequency part of the MR, which would be unrecoverable by the set PET acquisition system, is extracted and added to the PET image. This paper introduces a new application of the human vision system model in multispectral medical image fusion. The presented computer retina model is based on Difference-of-Gaussian operator. The proposed method is compared with the HIS, DWT, wavelet-based sharpening and *à trous* wavelet transform methods. Results showed that the retina-based image fusion method preserves more spectral and spatial features than other fusion techniques.

References

Burt, P.J., 1984. The Pyramid as a Structure for Efficient Computation. *In*: Rosenfeld, A. (Ed.), Multiresolution Image Processing and Analysis. Springer-Verlag, Berlin, p.6-35.

Burt, P.J., Kolczynski, R.J., 1993. Enhanced Image Capture Through Fusion. Int. Conf. on Computer Vision, p.173-182. [doi:10.1109/ICCV.1993.378222]

Choi, M., 2006. A new intensity-hue-saturation fusion approach

to image fusion with a tradeoff parameter. *IEEE Trans. on Geosci. Remote Sensing*, **44**(6):1672-1682. [doi:10.1109/TGRS.2006.869923]

Garzelli, A., Nencini, F., 2005. Interband structure modeling for Pan-sharpening of very high-resolution multispectral images. *Information Fusion*, **6**:213-224. [doi:10.1016/j.inffus.2004.06.008]

Ghassemian, H., 2001a. Multisensor Image Fusion by Multiscale Filter Banks. Proc. IEEE Int. Conf. on Image Processing.

Ghassemian, H., 2001b. A Retina Based Multi-resolution Image Fusion. Proc. IEEE Int. Geoscience and Remote Sensing Symp.

Goshtasby, A., 2005. 2-D and 3-D Image Registration for Medical, Remote Sensing, and Industrial Applications. Wiley Press.

Goshtasby, A., Nikolov, S., 2007. Image fusion: advances in the state of the art. *Information Fusion*, **8**:114-118. [doi:10.1016/j.inffus.2006.04.001]

Joshi, M.V., Bruzzone, L., Chaudhuri, S., 2006. A model-based approach to multiresolution fusion in remotely sensed images. *IEEE Trans. on Geosci. Remote Sensing*, **44**(9):2549-2562. [doi:10.1109/TGRS.2006.873340]

Kingsbury, N., 1999. Image Processing with Complex Wavelets. *In*: Silverman, B., Vassilicos, J., (Eds.), Wavelets: The Key to Intermittent Information. Oxford University Press, p.165-185.

Kolb, H., 1991. The Neural Organization of the Human Retina. *In*: Heckenlively, J.R., Arden, G.B. (Eds.), Principles and Practices of Clinical Electrophysiology of Vision. Mosby Year Book Inc., St. Louis, p.25-52.

Lewis, J.J., O′Callaghan, R.J., Nikolov, S.G., Bull, D.R., Canagarajah, C.N., 2004. Region-based Image Fusion Using Complex Wavelets. Proc. 7th Int. Conf. on Information Fusion. Stockholm, Sweden, p.555-562.

Li, Z., Jing, Z., Yang, X., 2005. Color transfer based remote sensing image fusion using non-separable wavelet frame transform. *Pattern Recog. Lett.*, **26**:2006-2014. [doi:10.1016/j.patrec.2005.02.010]

Mallat, S., Zhong, S., 1992. Characterization of signals from multiscale edges. *IEEE Trans. on Pattern Anal. Machine Intell.*, **14**(7):710-732. [doi:10.1109/34.142909]

Nikolov, S.G., Bull, D.R., Canagarajah, C.N., 2000. 2-D Image Fusion by Multiscale Edge Graph Combination. Proc. 3rd Int. Conf. on Information Fusion. Paris, France, p.16-22.

Nikolov, S.G., Hill, P., Bull, D.R., Canagarajah, C.N., 2001. Wavelets for Image Fusion. *In*: Petrosian, A., Meyer, F. (Eds.), Wavelets in Signal and Image Analysis. Kluwer Academic Publishers, the Netherlands, p.213-244.

Nunez, J., Otazu, X., Fors, O.I., Prades, A., Pala, V., Arbiol, R., 1999. Multiresolution-based image fusion with additive wavelet decomposition. *IEEE Trans. on Geosci. Remote Sensing*, **37**(3):1204-1212. [doi:10.1109/36.763274]

Petrovic, V.S., Xydeas, C.S., 2004. Gradient-based multiresolution image fusion. *IEEE Trans. on Image Processing*, **13**(2):228-237. [doi:10.1109/TIP.2004.823821]

Piella, G., 2003. A general framework for multiresolution image fusion: from pixels to regions. *Information Fusion*, **4**:259-280. [doi:10.1016/S1566-2535(03)00046-0]

Toet, A., 1990. Hierarchical image fusion. *Machine Vision Appl.*, **3**:1-11. [doi:10.1007/BF01211447]

Wang, Z., Ziou, D., Armenakis, C., Li, D., Li, Q., 2005. A comparative analysis of image fusion methods. *IEEE Trans. on Geosci. Remote Sensing*, **43**(6):1391-1402. [doi:10.1109/TGRS.2005.846874]

Zheng, Y., Essock, E.A., Hansen, B.C., Haun, A.M., 2007. A new metric based on extended spatial frequency and its application to DWT based fusion algorithms. *Information Fusion*, **8**:177-192. [doi:10.1016/j.inffus.2005.04.003]

Zhou, J., Civco, D.L., Silander, J.A., 1998. A wavelet transform method to merge Landsat TM and SPOT panchromatic data. *Int. J. Remote Sensing*, **19**:743-757. [doi:10.1080/014311698215973]